A comparative performance assessment of the hydrodynamic journal bearing lubricated with the oil and magnetorheological fluid

Quinci F.[a], Litwin W.[b], Wodtke M.[b], van den Nieuwendijk R.[a]

[a] *Bifröst Research and Development B.V., Molenvliet 34, 3961 MV Wijk bij Duurstede, the Netherlands*

[b] *Gdansk University of Technology, Faculty of Mechanical Engineering and Ocean Engineering, ul. Narutowicza 11/12, 80-233 Gdansk, Poland*

Abstract

This work presents investigations results of journal bearing lubricated with magnetorheological fluid that is activated by a local constant magnetic field to vary both the local flow resistance and pressure. The bearing performance is assessed via Finite Element Modelling (FEM) and results are corroborated by experimental tests. The FEM model uses the ideal Bingham model to describe the fluid film. A dedicated test rig is used to evaluate the hydrodynamic behavior of the bearing with magnetorheological fluid, and results are compared with the same geometrical bearing lubricated with the oil. Thicker fluid films at low speeds, beneficial pressure distribution and higher friction losses at all operating conditions are observed in the bearing with magnetorheological fluid compared to the oil lubrication.

Keywords: hydrodynamic journal bearing, magneto-rheological lubrication, experimental investigations

1.   Introduction

Oil lubricated sliding bearings are widely used in high speeds rotating and reciprocating machines such as turbines and compressors due to their good load carrying capacity and durability [1,2].

Throughout the years, bearings have been improved since their initial conception [3], but still the energy losses due to viscous friction and system failure are considerable. The lubricated bearing in its simplest form consists of two parts in relative motion with a lubricant in-between. Depending on the application and its working velocity range, one can choose a hydrodynamic bearing for high speed applications to gain benefits in system alignment, friction and damping [4–6]. This bearing configuration supports the rotating shaft through a pressurized oil film [7]. However, at low speeds, the lubricating film might not be able to sustain the shaft load anymore, leading the bearing surfaces into physical contact with excessive friction and wear, and ultimately compromising the integrity of the system. In case the system operates at low speeds, hydrostatic bearing are a suitable option since they are externally pressurized, ensuring a separation gap between bearing surfaces [8]. Hydrostatic bearings use failure sensitive high-pressure supply pumps to pressurize the lubricant and lift up the shaft at critically low speeds. Once the pump fails, high wear in the bearing is generated as its performance in the hydrodynamic regime is very poor due to the unfavorable geometry related to the presence of pockets in the sliding surface [9,10]. Despite the wide selection of lubricated bearings nowadays available, the optimization of surface textures and lubricants have only led to small improvements, and relevant

technical limitations still remains. Interesting developments are seen in the field of tribotronics [11] with the introduction of smart fluids to actively control vibrations and damping in dampers [12], bearings [5,13–17] as well as in brakes applications [18]. Smart fluids like magnetorheological (MR), electrorheological (ER) and ferrofluid (FF) contain magnetic iron particles dispersed in a carrier oil, but they differ in particle size and the way each of them responds to an imposed excitation. Both MR and ER fluids are referred as pseudo-plastic or Bingham since they behave as rigid bodies at low stresses but flow as viscous fluids at high stresses when excited by a magnetic or an electric field, respectively. In these fluids, suspended particles tend to sediment over time, but their viscosity can vary of several orders of magnitude in fraction of milliseconds, making them more appealing than conventional lubricating fluids for applications like lubricated bearings [19–22]. On the other hand, FFs are colloidal liquids that contain ferromagnetic nanoparticles coated with surfactant to keep the particles in suspension by Brownian motion, which show non-Newtonian effects in presence of magnetic field [23,24]. Among all the discussed smart fluids, MR seems to be the most promising for heavy duty rotary machines due to their ability to generate greater fluid forces [25] since the yield stress is about tenfold higher than the yield stress in ER fluids [22]. Besides, ER fluids must be degassed and pressurized to avoid cavitation, which problem is far less prominent in MR fluids [26]. In case of FFs, they do not meet the requirement of viscosity change for lubricated bearings since only small viscosity changes occur under the imposition of a magnetic field [5,19,27]. It is worth to mention that a limited number of works that deal with bearings lubricated with MR is available in literature [25]. In [28], a MR fluid was used in a hydrostatic bearing to keep the gap constant when the pay-load was varied. They proved the system to react faster to changes in applied loads than the external valve base system since the MR fluid acts right inside the gap. The work of [5] compared the performance of a hydrodynamic bearing lubricated with MR fluid against one lubricated with FF. The Authors concluded that the MR fluid is a better candidate for active control than the FF due to the greater change in viscosity under magnetic field. The numerical study of [25] on hydrodynamic bearing confirmed the positive contribution of MR lubricant to the bearing load-carrying capacity under the influence of a magnetic field. Conventional bearings change their flow resistance by local changes in the surface geometry, so called local texture, which cannot be varied during operations [10]. On the contrary, bearings lubricated with MR fluid are able to tune the viscosity during operations by the imposition of a magnetic field, thus creating a local change in flow resistance, so named MR texture [29]. A negative side associated with the use of smart fluids as lubricants is the increase in friction, which causes higher torques and therefore greater system power consumption [5,25].

According to provided literature, there are only few works investigating the performance of hydrodynamic bearings lubricated with MR fluids, hence there is still a gap in knowledge concerning their operational performance, especially when trying to make a direct comparison to other bearings types. The goal of this research is to investigate a full size hydrodynamic journal bearing under operation with two types of lubricants: MR fluid and conventional mineral oil. To do so, an experimental setup to verify the effects of using a MR fluid in a hydrodynamic journal bearing during operation at different speeds and loads was used. Results of the experimental research (e.g. eccentricities, bearing friction losses, film pressures), complemented with numerically calculated bearing parameters, allowed to directly compare the bearing performance depending on the used lubricant. Based on the results analysis,

the main differences between the operational behavior of the bearing lubricated with MR fluid and with mineral oil were identified and discussed in detail.

2.   Materials and methods

Experimental tests of the bearing lubricated with two different types of lubricants under hydrodynamic regime were planned. First, the journal bearing was lubricated with mineral oil, further called "reference bearing", with rheological properties of the oil reported in Tab. 3 and Fig. 3. Then, the bearing was cleaned and lubricated with a MR fluid, further called "tested bearing". This was realized without disassembling the bearing and the rest of the equipment in order to keep the alignment of components constant between tests and thus in repeatable assembly conditions. Supplementary to experiments, bearing parameters were also evaluated theoretically with the aid of FEM models for both lubricants, which allowed together to confirm the general validity of the applied theory and also to expand analyses over the bearing parameters not available experimentally.

Tested bearing

A hydrodynamic plain journal bearing of 100 mm shaft diameter was selected as an object of the research. The bearing bush was made of CuSn7Zn4Pb7-C bronze (2.1090 / RG7). The main geometrical parameters of the tested bearing are reported in Tab. 1 (with the proportion L/d = 2, typical for stern tube bearing of the main shaft in ships, often lubricated by oil [6] or water [30,31]). The bearing was lubricated with 4 cylindrical inlets positioned horizontally (two inlets at 90° and two inlets at 270°, coordinate system is shown in Fig. 1, inlets marked in Fig. 2) and distanced 25 mm from the bearing ends (shallow grooves were machined between inlets to connect them and assure better flow conditions into the gap).

Tab. 1. The main geometrical parameters of the tested bearing; also used in the FEM model.

Variable	Symbol	Value
Bearing diameter	d	100 mm
Bearing length	L	210 mm
Diametral clearance	c	0.3mm
Magnet diameter	D	16 mm
Gap between magnets	g	D/4

The bearing was equipped with 35 permanent magnets of diameter D = 16 mm. The magnets were close to the bush sliding surface, and the distance to the surface was only 0.85 mm. In Tab. 2, technical details of the magnets are shown. The magnetic pattern generated by magnets is presented in Fig. 2. The criteria for selecting the parameters of magnets were based on the preliminary bearing properties assessment in connection with the behavior of selected MR fluid under magnetic field. The magnetic pattern is vertically symmetric since it is assumed, that bearing lubricated with MR fluid should be able to operate with the same operational parameters irrespective to the direction of the shaft rotation.
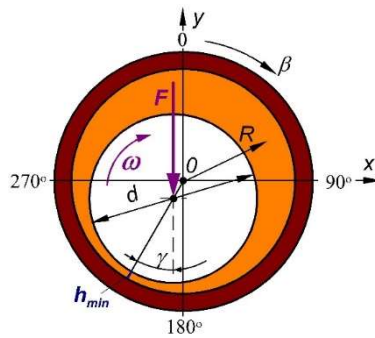
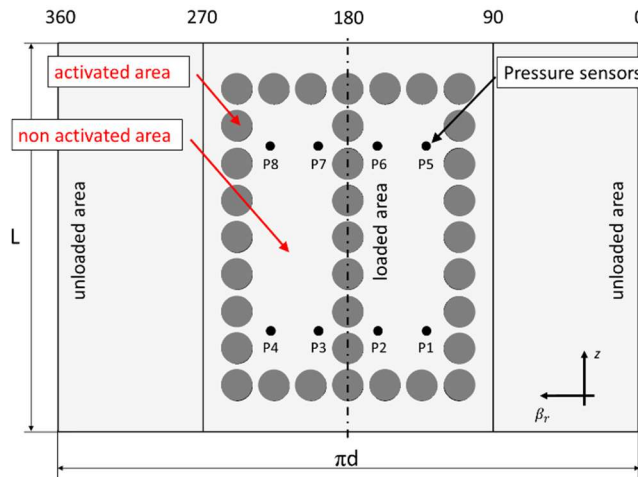*Fig. 1. Schematic of the bearing side view (cylindrical coordinate system).*

Fig. 2. Unfolded journal bearing with magnetic buttons (grey circles) on bearing bush perimeter.

Tab. 2. Technical datasheet of permanent magnets

Material	NdFeB/N35
Height (magnet diameter/2)	8 mm
Coating	Ni
Flux density inside the magnet	1.17 T
Flux density on surface	0.38 T (~300 kA/m)
Max operating temperature	80 ˚C
Dead weight	11.46 g
Holding force on iron	62.1 N
Weight the magnet can lift	6.33 kg

Material properties of lubricants

For oil lubrication, the stern tube mineral oil SAE 30 class was used. In case of MR lubrication, the lubricant consisted of iron particles dispersed in a hydrocarbon carrier. Measured variations of the MR fluid viscosity for different magnetic fields are compared as a function of speed and temperature in Fig. 3. Tab. 3 summarizes the material properties of both MR and SAE 30 lubricants.

Tab. 3. Properties of the SAE30 oil and MR fluid used in tests.

	Properties	Value
SAE 30 mineral oil	Dynamic viscosity at 40-80 ℃	0.088-0.017 Pa·s Fig. 3

4

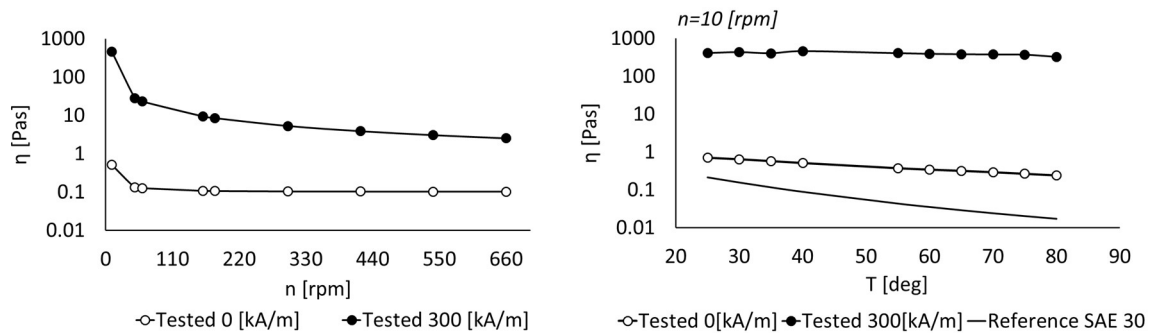|	Density at 15 °C	0.890 g/ml
MR fluid	Operating temperature	-40°C to 140 °C
	Density	2.49 g/cc
	Packing fraction by weight	70 %
	Colour	Grey
	Flash point	> 190 °C
	Dynamic viscosity (n,T)	Fig. 3
	Yield stress at 0-300kA/m	9.4-13500 Pa

Fig. 3. Viscosity in function of speed (10-660 rpm) for magnetic fields of 0-300 kA/m and constant temperature of 40 °C (left); Viscosity of MR fluid in function of temperature for magnetic fields of 0-300 kA/m and constant speed of 10 rpm and oil SAE 30 at same speed (right).

In Fig. 3, the viscosity of the MR fluid exhibited a strong dependence on speed, specifically it decreased with increasing speed. The highest viscosities, irrespective of applied magnetic field, were measured at low speeds. It is noteworthy that the viscosity measured in the presence of the magnetic field was around three orders of magnitude higher than the viscosity measured without it. Much smaller variations of MR fluid viscosity were observed with temperature (right-hand side of the figure). In the absence of magnetic field, the MR fluid showed a similar decreasing trend in viscosity with increasing temperature than the oil lubricant, but less pronounced. Once the magnetic field was applied to the MR fluid, its viscosity became practically independent upon temperature. For completeness, in Fig. 3 only data at 300 kA/m were reported since this was the magnetic field magnitude at the surface of the magnets used in the tested bearing.

Experimental setup

A schematic of the test stand used in this research work is shown in Fig. 4 and 5. The main shaft of the test stand is supported by two self-alignment ball bearings. Between them, there is a bearing test unit (fig. 4). An electric motor with reduction gear and AC controller were used for the drive. It has a 5.5 kW power output and a starting torque of about 160 Nm. On the main shaft (1), the tested bushing (4) with magnets (m) was mounted in a massive housing (2). Between the tested bush and the housing, an intermediate sleeve (3) was used. The lubricating liquid was supplied to the bearing by cylindrical inlets and axial grooves (L), which were machined at the bearing sliding surface. The lubricant outflowing from the gap at the bearing sides passed to the drain lines through the holes manufactured in both side

5

ends of the housing. Shaft was sealed with sealing rings assembled in covers (5) to protect against leakages. The load was exerted by a hydraulic cylinder via a hydrostatic bearing (6). Oil pressure measurement in the hydrostatic system was used to adjust and control the load applied to the bearing. The separation between the system exerting the load and the test stand housing by means of a hydrostatic film, assured self-aligning and enabled precise measurements of the friction force with the use of a cantilever beam (200 mm long) and a force sensor (a). The recorded data were used to obtain the bearing friction torque, and consequently the friction coefficient. Unfortunately, this support method had also a disadvantage. During the tests, there was no control over the position of the bushing axis with respect to the shaft axis. In fact, the bush operated as self-alignment sliding bearing.
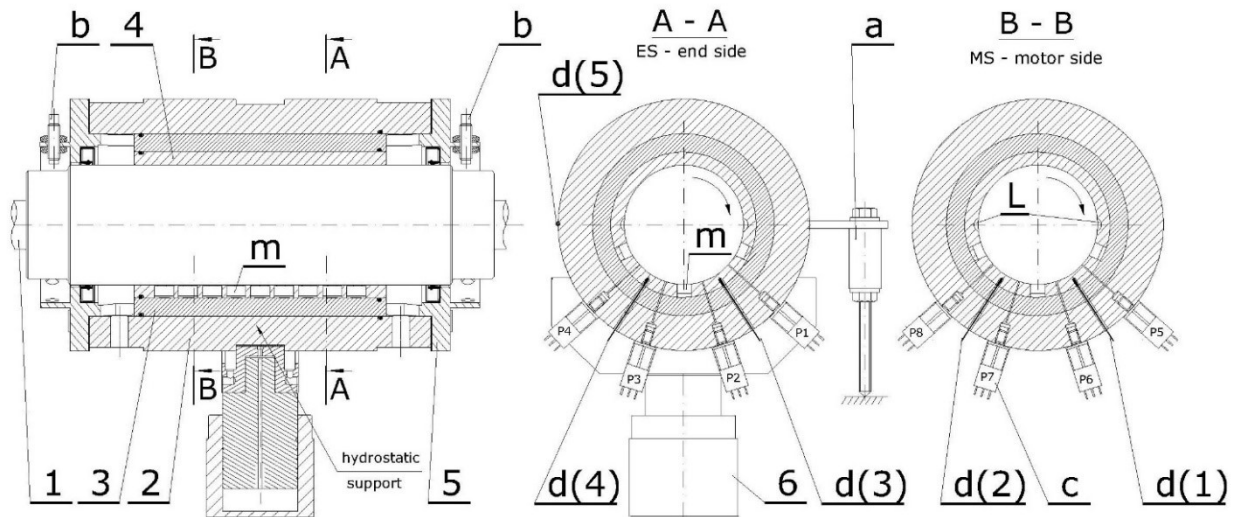

Fig. 4. Test rig schematic view; 1-main shaft, 2-external bush sleeve, 3-intermidiate bush, 4- bronze bearing bush, 5-side cover with seal ring, 6-load hydraulic jack, a-friction torque gauge, b-proximity sensors, c-pressure sensors, d-thermocouple, m- permanent neodymium magnets.

The bearing sleeve was equipped with five type K thermocouples (OD 1 mm) placed in two cross-sections (A-A plane → d(3), d(4) and d(5), B-B plane → sensors marked d(1) and d(2), see Fig. 4). The thermocouples were fixed in radial blind holes, 2 mm under the bearing sliding surface. Moreover, two additional thermocouples were applied to monitor lubricant temperature at inlet and outlet. The assessed accuracy of the measurements using the applied thermocouples was ± 0.5 °K. Lubricant flow through the bearing was adjusted using hydraulic valve and controlling inlet pressure. During all tests, the starting temperature of the lubricating liquid was 23±2 °C, the same as the ambient temperature. A view of the test stand under operation is presented in Fig. 5.

6

Fig. 5. The test rig during tests.

In addition to temperature sensors, pressure sensors (8 sensors, in two cross sections, see Fig. 4) were installed in the sleeve, with the holes (diameter 1 mm) drilled across its wall. To measure the relative shaft position in reference to the sleeve, eddy current distance sensors (two for each direction at both bearing ends) were used. All measured parameters were collected with the use of A/D data acquisition system, PC computer and A/D card. In Tab. 4, accuracy of sensors utilized in experimental tests are given.

Tab. 4. Bearing data, working conditions and details of measurement sensors.

Sensor	Accuracy
Pressure strain gauge sensors (8 pcs.), range 0÷6 MPa,	*±0.3% FS*
Friction torque measurements – strain gauge sensor with amplifier, range 0-100 N	*±0.5% FS*
Distance touchless measurements – proximity probes – with analog output	*±1% FS*
Temperature measurements – K thermocouples	*± 0.5 K*

For tests with mineral oil, the typical hydraulic supply system unit with 20 litters tank, gear pump, valves and internal warming up system was used. To safely use the MR fluid, a different lubricant supply hydraulic system was implemented, consisting of a cavity pump and a tank with a mixer to assure a homogenous dispersion of iron particles in the MR carrier during test. A cavity pump was selected for its ability to pump fluids with high viscosity and particles content, hence suitable for pumping the MR fluid (10 µm particles size).

Numerical model

Similarly to [10], the performance of the tested bearing was assessed through a FEM platform (COMSOL Multiphysics® 5.5). The Bingham plastic is used to capture the rheological behavior of the MR lubricant, while its flow is modelled with the Reynolds equations derived from the standard thin film fluid flow assumptions [20,25,32]. The schematic in Fig. 2 shows the unfolded journal bearing with an axisymmetric rectangular rheological texture consisting of a total of 35 circular magnetic buttons (Tab. 2).

For both tested and reference bearings, the fluid film height h is defined according to Eq. 1, where the eccentricity e is the relative position of the shaft with respect to the bearing. Eccentricity is zero when both shaft and bearing centers match, and one when the shaft touches the bearings. The variable β stands

for the angular coordinate in the bearing, while γ represents the angular offset where the lubricating film has its minimum h_{min} (Fig. 1).

$$h = c(1 - e\cos(\beta + \gamma))$$
<div align="right">Eq. 1</div>

From the computed pressure in the lubricating film, the load carrying capacity F_y in the vertical y-direction is obtained, which equals the total load carrying capacity F_{res} of the bearing (Eq. 2).

$$F_{res} = F_y = \iint_s p\cos(\beta)\, dA$$
<div align="right">Eq. 2</div>

The friction force F_f generated in the bearing is expressed by Eq. 3. The parameter τ_β is the local stress required to achieve the desired relative motion of the two surfaces. The friction coefficient f in Eq. 4 is obtained as the ratio between the load capacity F_{res} in Eq. 2 and the friction force of the bearing F_f in Eq. 3.

$$F_f = \iint_s -\tau_\beta - \frac{h}{2}r\frac{\partial p}{\partial \beta}\, dA$$
<div align="right">Eq. 3</div>

$$f = \frac{F_{res}}{F_f}$$
<div align="right">Eq. 4</div>

The rheological behavior of the MR lubricant is described in Eq. 5, where the stress τ in the fluid is function of the shear rate $\dot{\gamma}$. Both the yield stress and the viscosity of the fluid are dependent on the magnetic field H. The parameters used in simulations and their values are reported in Tab. 1 and Tab. 3.

The mathematical model used to describe the flow of the MR lubricant in-between the two moving surfaces is extensively discussed in [32]. In the model, the thin film flow is modelled by means of a modified Reynolds equation that uses the exact Bingham plastic material.

$$|\vec{\tau}| = \tau_0(H) + \eta(H)|\vec{\dot{\gamma}}|$$
<div align="right">Eq. 5</div>

Tab. 5 summarizes the applied viscosity conditions for reference and tested bearings.

Tab. 5. Viscosity conditions applied to reference and tested bearings.

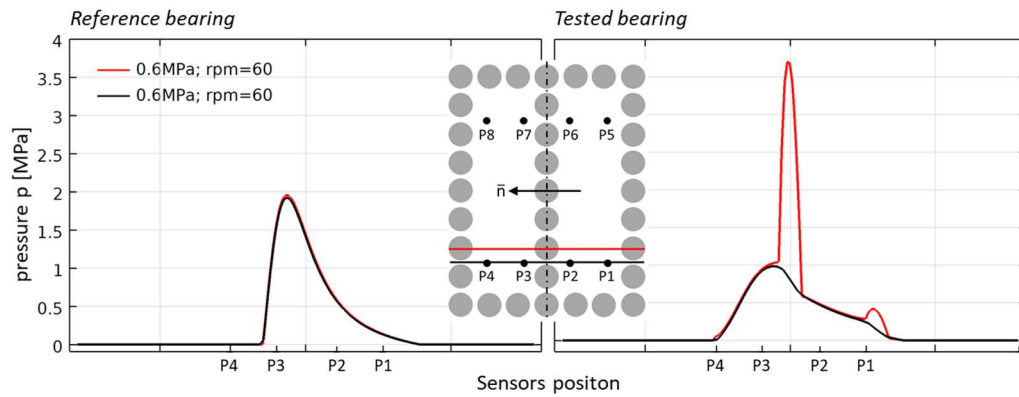|	*Non-Activated areas*	*Activated areas (magnets)*
Stern tube mineral oil SAE 30	$\eta = 0.088\, Pa \cdot s$ *(at 40°C)*	*Switched off*
MR fluid	$\eta_{H=0kA/m}$ $\tau_0 = 9.4Pa$	$\eta_{H=300kA/m}$ $\tau_0 = 13500Pa$

Fig. 6. FEM pressure profiles taken at the sensors line (black line through sensors) and magnet line (red line through magnets) for the tested and reference bearings. For the reference bearing simulations, magnets were switched off, and mineral oil viscosity was applied uniformly to the whole bearing surface.

Fig. 6 shows FEM pressure profiles for reference and tested bearings at 60 rpm, for an applied load of 0.6 MPa and for a clockwise rotation of the shaft, as in the experiment. Pressures peaks for the tested bearing were located over the magnets. On the other hand, a more homogeneous pressures distribution was predicted for the reference bearing, with maxima slighly to the left of the centre axis of the loaded area (180 deg in Fig. 2). At magnet locations of the tested bearing, the predicted pressure peak was nearly twice in values compared with the maximum pressure measured in the reference bearing.

Test conditions

The bearing, irrespective of the applied lubricant, was tested at the same operating conditions. In this scenario, the bearing performance is solely dependent on the physical properties of the lubricant, thus allowing a direct comparison between different lubricants. Three levels of specific pressure were selected (0.2; 0.4 and 0.6 MPa) and six levels of shaft speed (60; 180; 300; 420; 540 and 660 rpm).

Before every test, an important action was required in preparation for the measurements, that is the unit warm-up (Fig. 7). The bearing warm-up phase could take from 20 to 40 minutes depending on the different combinations of loads and speeds. It is important to mention that the bearing test unit is a very sensitive system, which means that even small changes in operating conditions produced sudden changes in temperature.

Additionally, initial warm-up in the tank was possible only for the oil, but not for the MR fluid. The reason is that the bearing lubricated with MR required different and more specific supply and mixing auxiliary systems than the oil JB because of the presence of iron particles in the MR carrier.

The operational, stable temperature of the bearing unit lubricated by MR liquid was expected to be in the range 35-45 °C, which fact was confirmed by measurements in Fig. 7-b. Instead, the oil lubricant was warmed up to a temperature of about 35°C (Fig. 7-a). Difference in temperatures between the tested and reference bearings could be attributed first to the presence of iron particles in the MR fluid, then to its smaller flow compared to oil lubricant. Lubricant inlet pressure was always constant 0.15 MPa.
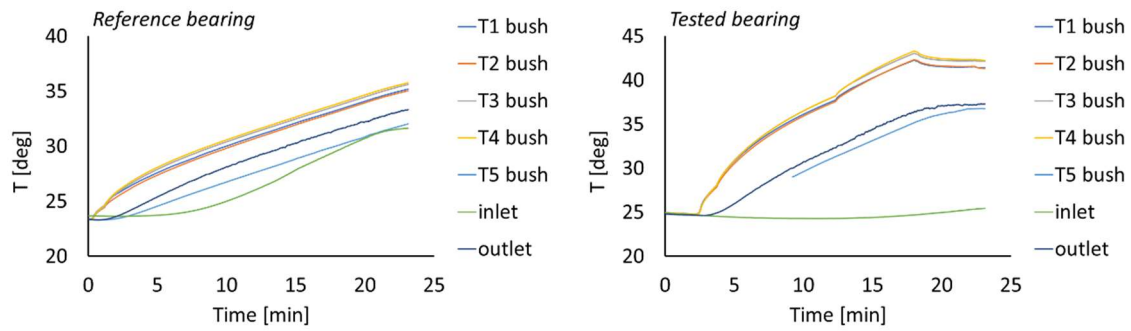
Fig. 7. Warm-up phase diagram acquired for oil (a) and MR lubricants (b).

3. Results & discussion

Instrumentation of the bearing and the test rig allowed to monitor the bearing performance during tests at defined levels of shaft speed and radial load. Results presented in this section are averaged values obtained from three identical series of measurements for the bearing lubricated with both lubricants to avoid random mistakes in measurements.

Shaft center orbits trajectories were used to estimate locus and eccentricities, which parameters are directly related to the film thickness and thus bearings working regimes. The bearing load capacity and pressure distribution were estimated by pressure sensors. Friction power losses and thermal bearing behavior were assessed through friction torque and temperature measurements.

Locus and eccentricties

Locus were estimated based on shaft canter orbits trajectories data gathered through proximity sensors placed at the two ends of the bearing (Fig. 4– component 'b'); the sensor located close to the motor is referred to as "Motor Side" (MS), while the other sensor is named as "End Side" (ES). Besides, trajectories were also used to compute bearing parameters such as eccentricity and orbit location attitude angle (Fig. 1).

Experimental and FEM bearing locus plots at different speeds for both reference and tested bearings are shown in

Fig. 8. In the figure, all load and speed cases were collected. The three points, being part of a specific speed line, denoted three load levels. Specifically, the point located nearest to the bearing center (eccentricity 0) is the result of 0.2 MPa, while the point located closest to the sleeve surface (eccentricity 1) is the result of 0.6 MPa.

In general, FEM and experimental results show a good agreement in trends. The transition from boundary and mixed to full film lubrication in both reference and tested bearings, and for both FEM and experiments, could be seen by the motion of locus curves towards the eccentricity value of 0 with increasing speeds (

Fig. 8). The 0 eccentricity value means that bush and shaft centers are coincident.
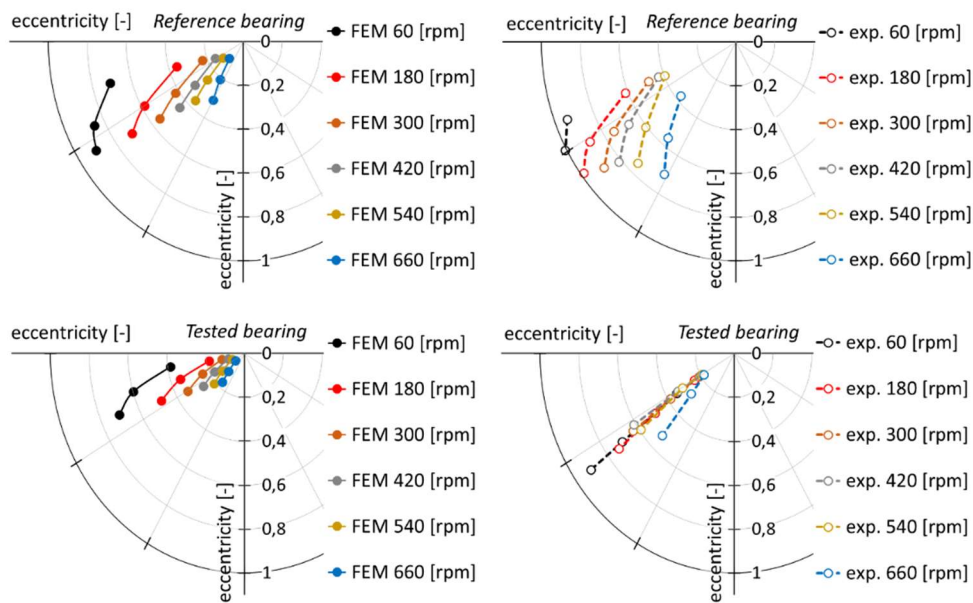
10

Fig. 8. Locus plots for MR and oil lubricated journal bearings at different speeds. FEM results are showed in the left column, while experimental results in the right column.

Besides, as expected, in both tested and reference bearings the lubrication film becomes thinner with higher applied loads, specifically from 0.2 to 0.6 MPa as shown in Fig. 9.

Clear differences in lubrication properties between tested and reference bearings do exist, as evidenced by the comparison between eccentricity values at different speeds and loads (Fig. 9).

The locus curves of the reference bearing are shifted towards higher eccentricity values compared to the tested bearing (

Fig. 8), which is for the latter a clear indication of a thicker lubrication film. This difference is also clearly visible in Fig. 9, where eccentricities for the tested bearing present lower values for each load and speed. Based on these results, it can be stated that the tested bearing might have already reached the hydrodynamic regime at the lowest speed of 60 rpm, which is not the case for the reference bearing. For the reference bearing, the lubrication regime seemed to be either mixed or boundary since the eccentricity measured in the experiment was very close to value 1 at 60 rpm (at 0.4 and 0.6 MPa).
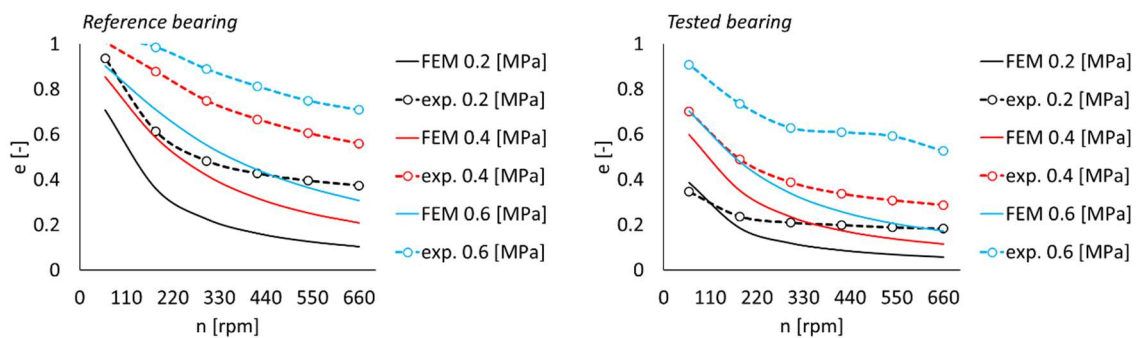

Fig. 9. Eccentricity at different speeds and applied loads for reference and tested bearings.

As mentioned earlier, FEM and experiments for both tested and reference bearings followed similar trends although values differed. In Fig. 10, which shows eccentricities over speeds at constant applied load (0.2 MPa) for tested and reference bearings, the gap between experiments and FEM increased with

11

increasing speed. For the reference bearing, the percentage difference between experiments and FEM is 28-113 % for a speed range 60-660 rpm, while for the tested bearing is 9-73 % for the same speed range. Therefore, FEM predictions seem to be more accurate for the tested bearing than the reference bearing.
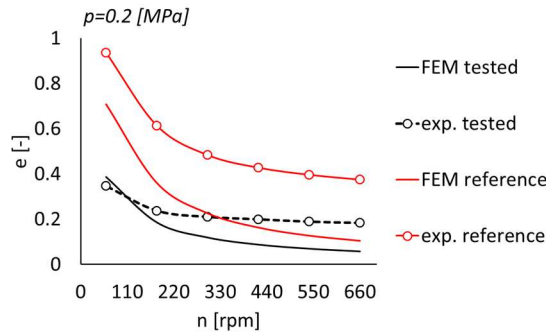

Fig. 10. Eccentricity comparison between FEM and experimental results for an applied loads of 0.2MPa.

Fig. 10 also shows lower eccentricities for the tested bearing than the reference bearing, which is again an indication of a thicker lubricant film for the latter. Thick films at low speeds are desired since it is a sign of the presence of hydrodynamic regime at critical operating conditions, where wear and surface damage become a substantial problem, probably leading to early bearing failure. Therefore, the presence of thicker films at low speeds in the tested bearing means that it can be either loaded more at same geometry or smaller in size at same applied load, when compared to the reference bearing,

Pressures

Fig. 11 presents experimental and FEM pressure results for tested and reference bearings at three different speeds and for an applied load of 0.6 MPa. The film pressure was measured with pressure sensors P1, P2 , P3 and P4 (Fig. 4, section A-A) that were located at respectively 141, 197, 193, and 219 degrees. Besides, only one load and side of the bearing was considered for illustrative purposes, since trends and values were similar between sides and loads.

The experimentally recorded fluid film pressure under a low speed of 60 rpm was higher in the tested bearing compared to the reference bearing. The pressure profile of the tested bearing seemed to better represent a typical hydrodynamic regime when compared to the reference bearing, with maximum value in proximity of the divergent zone. This could be the evidence of a proper hydrodynamic action of such bearing design especially at low speed and high load conditions. On the other hand, there are no significant differences in values and trends between experimental fluid pressure films of tested and reference bearings at higher speeds (180 and 660 rpm).
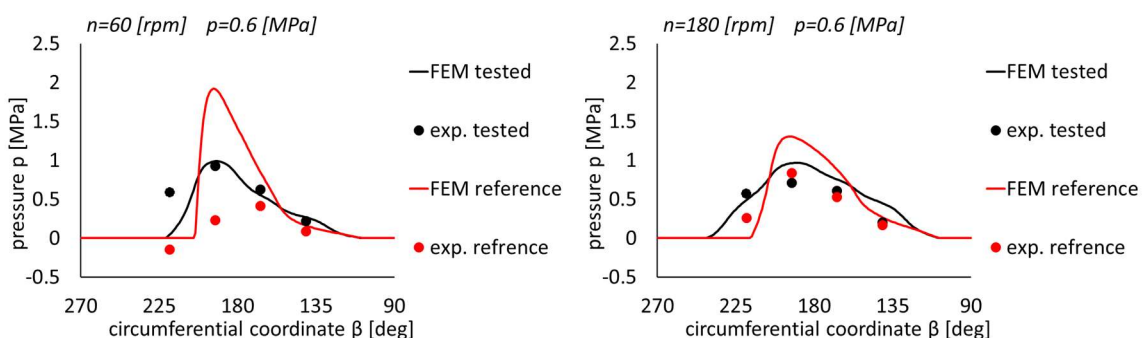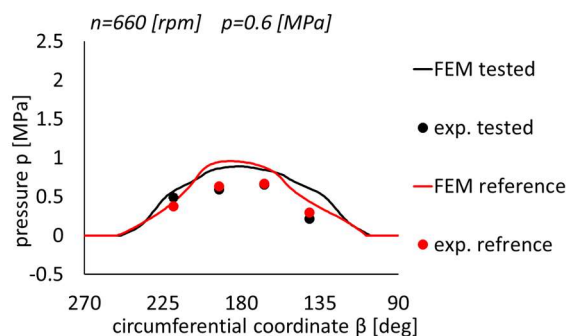
Fig. 11. FEM and experimental film pressure results for tested and reference bearings, three different speeds and an applied load of 0.6 MPa, are reported.

At low speed, that is 60 rpm, the experiment and simulation for the tested bearing were in good agreement, while slightly larger difference in values was measured at 660 rpm. The reference bearing operated at low speed (60 rpm) presented low values of hydrodynamic pressure, which trend disagreed with the theoreticaly predicted gap pressure, not only in terms of values but also in terms of obtained profile. Simultaniously, much better agreement was observed in measured and simulated pressures values for higher speeds.

This discrepancy in pressure profiles for the reference bearing at low speed (60 rpm) and high load (0.6 MPa) could be explained by means of locus results in

Fig. 8. The measured eccentricity for this specific operating condition was 1, which means that the bearing was not operating in full hydrodynamic regime, but more likely in mixed lubrication with the load partially carried out also by asperity contacts between shaft and bush.

Theoretical results were obtained with the assumption of hydrodynamic operation, perfect geometrical shape of the bearing components (shaft and bush) and absence of system imbalance. However, in conditions of low speed (60 rpm) and high load (0.6 MPa), the hydrodynamic effect is strongly limited and dependent by the minimum thickness of the lubrication film oil. Likely, the hydrodynamic effect was not obtained for the reference bearing in experimental tests under such operating conditions due to bore shape deviations (ovality, waveness etc.) or system imbalance. Both effects are able to reduce effectivenes of hydrodynamic lubrication. For that reason, measured and simulated pressure profiles dissimilarity was not so evident for operating conditions that promoted more the hydrodynamic effect and consequently could reduce (accommodate) the influence of sleeve shape deviations or imbalance. The pressure measurement at speed of 180 rpm and load of 0.6 MPa confirm that statement since experimental and simulation values are in good agreement, confirming the presence of hydrodynamic effect. To conclude, the FEM model can solely simulate the bearing beahviour in hydrodynamic regime, but not mixed regime and this could be the reason for higher predicted pressures at low speeds (60 rpm) and the better agreement at intermediate (180 rpm) and high (660 rpm) speeds.

On the other hand, we can not see higher values of measured coefficient of friction for tested bearing (Fig. 12). This could be due to the fact that the plotted coefficients of friction were avaraged and due to the relatively low value of the friction power under oeprating condition at low speed (60 rpm). In addition, according to the Stribeck curve, close to the transition point between lubrication modes, the coefficient of friction for hydrodynamic and mixed lubrication does not differ too much.

13

Besides, a further explanation is given with aid of Fig. 6, where peaks in the tested bearing were predicted over the magnets, while in the reference bearing to the left of the centre axis (clockwise shaft rotation), precisely in in proximity of sensor P3. Therefore, it is possible that pressure sensors were not measuring the highest pressures in the reference as well as tested bearings.

Slightly away from peaks (Fig. 6 and Fig. 11), the tested bearing at 60 rpm showed a plateau-like pressure distribution across the bearing, while the reference bearing presented a more sudden drop. This plateau-like shape of the pressure allowed the tested bearing for a more efficient use of the available surface area, leading to an improved load carrying capacity, as registered by the pressure sensors in the experiment. Therefore, a smaller bearing able to carry the load can be envisaged.

Coefficient of friction

Bearing load was exerted with the use of hydrostatic support in experimental setup. This, besides of application of the radial load, allowed practically to eliminate movement resistance of the bearing housing relative to the shaft when loaded. Hydrostatic lubrication assured full separation of the bearing housing from the hydrostatic support with the use of fluid lubrication between elements and thus allowed to measure only losses in the tested bearing (composed with power losses in the bearing gap due to lubricant shearing and power losses due to friction in the sealings rings) by means of force sensor (a in Fig. 4).

Measured friction forces (fig. 4. commponent 'a') were recalculate on bearing coefficient of friction taking into account applied load and geometrical parameters of the system (bearing diameter and force sensors distance from bearing center).
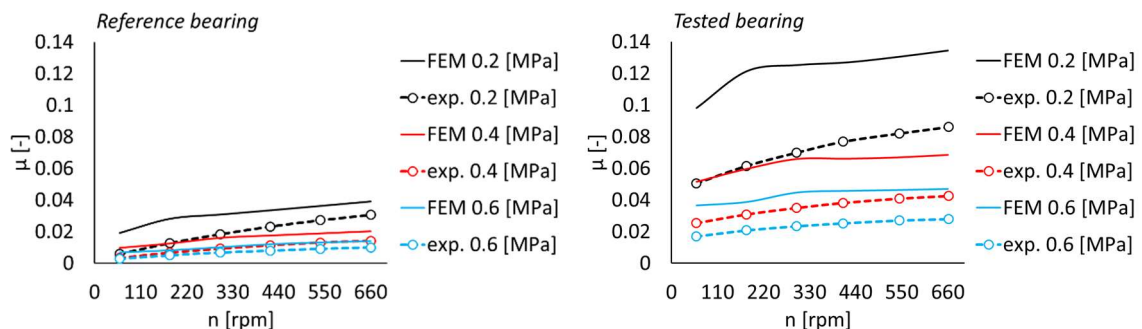

Fig. 12. Coefficient of friction at different speeds and applied loads for reference and tested bearings.

In Fig. 12 one can notice, that friction losses were measured higher for the tested bearing compared to the reference bearing, and similarly these losses increased with increasing speed for both tested JBs.

The significant losses recorded in the experiment for the tested bearing are probably connected with the increase of the local viscosity due to the Bingham effect that is caused by the permanent magnetic field. The magnetic patern, which depends on the positon of magnets underneath the bearing surface (activated areas in Fig. 2), and the average size of particles in the MR fluid have both a direct impact on the amount of losses due to friction. The suspended iron particles in the MR fluid were on average 10 μm in size, while the thinnest simulated film thickness was of 40 μm at 60 rpm. It is likely that during specific operating conditions of the tested bearing, the gap between shaft and bearing was filled with several layers of particles at areas where the magnetic field was maximum, increasing friction losses as well as causing surface damage, mainly abrasive wear.

4. Conclusions

Results clearly indicate that the tested bearing, which is lubricated with MR fluid, presents higher potential than the reference oil bearing. The most important feature evidenced in the tested bearing is the larger film thickness measured at low speed. However, friction losses at high speeds are a problem that still needs to be investigated. It is worth to mention that in this work, permanent magnets were used, thus the magnetic field was constant in all experimental conditions. A possible way to reduce losses foresees the use of electromagnets [33,34], which technology introduces the concept of controllable film thickness. This active control, which is the possible next development step of this work, could be used to obtain a thicker lubrication film at low speed by increasing the viscosity of the MR fluid through a strong magnetic field. Therefore, a better separation between bearing surfaces could be expected.

On the other hand, the magnetic field could be turned off or lowered at high speeds to reduce the MR fluid viscosity and thus to decrease friction losses. Moreover, the active control of the hydrodynamic bearing properties is also possible by changing the magnetic field when both shaft speed and orbit are acquired and processed in real time. This concept is similar to the control of active magnetic bearing in which the shaft levitate moved by an electromagnetic field, and its position is controlled by proximity sensors [35].

In the standard MR fluid utilized in tests, neither the carrier nor the particle size were optimized for this specific application. Both visual and optical microscope inspections of the bearing surfaces after test (pictures not included), showed more severe abrasion marks in the brass bush than in the steel shaft, which is expected since the former is a softer material. Therefore, there is a necessity of using a tailor-made MR fluid with possibly smaller particles and anti-wear additives. Besides, new bearing coupling materials that work in harmony with a new MR fluid must be investigated. To this end, dedicated wearing tests of various sliding pairs are planned in future. The next investigations have also to account for the particles sedimentation process, the necessity of fluid mixing and the problem of particles that might get stacked in the lubricating system due to the influence of magnetic forces coming from ferromagnetic components.

To further improve the test rig measurement capabilities, one could consider a more precise friction losses measurement system, capable of assessing the friction only in the bearing and neglecting the losses in the sealing systems.

5. Acknowledgments

6. Credit authorship contribution statement

Alphabetic order:

Federico Quinci: Research inspiration, Writing - original draft, Calculations, Theoretical model creating, Results processing and analyzing.

Wojciech Litwin: Experimental investigation, Writing - review & editing ,Resources, Data curation.

Michal Wodtke: Experimental investigation, Writing - review & editing, Resources, Data curation Conceptualization, Methodology, Investigation, Resources, Visualization.

Roy van den Nieuwendijk: Writing - review & editing, Resources, Data curation Conceptualization, Methodology, Investigation, Resources, Visualization.

7. Declaration of competing interest

The authors declare that they have no known competing financial interests or personal relationships that could have appeared to influence the work reported in this paper. (the same like in recent paper)

8. References

[1]   Patel NS, Vakharia DP, Deheri GM. A study on the performance of a magnetic fluid based hydrodynamic short porous journal bearing. J Serbian Soc Comput Mech 2012;6:28–44. https://doi.org/10.5402/2012/603460.

[2]   Hashimoto H. Optimization of Oil Flow Rate and Oil Film Temperature Rise in High Speed Hydrodynamic Journal Bearings. In: Dowson D, Taylor CM, Childs THC, Dalmaz G, Berthier Y, Flamand L, et al., editors. Tribol. Energy Conserv., vol. 34, Elsevier; 1998, p. 205–10. https://doi.org/https://doi.org/10.1016/S0167-8922(98)80075-8.

[3]   Myshkin NK, Goryacheva IG. Tribology: trends in the half-century development. J Frict Wear 2016;37:513–6.

[4]   Childs PRN. 5 - Journal bearings. In: Childs PRNBT-MDEH (Second E, editor., Butterworth-Heinemann; 2019, p. 167–230. https://doi.org/https://doi.org/10.1016/B978-0-08-102367-9.00005-6.

[5]   Urreta H, Leicht Z, Sanchez A, Agirre A, Kuzhir P, Magnac G. Hydrodynamic bearing lubricated with magnetic fluids. J Intell Mater Syst Struct 2010;21:1491–9. https://doi.org/10.1177/1045389X09356007.

[6]   Litwin W. Experimental research on marine oil-lubricated stern tube bearing. J Eng Tribol 2019;233:1773–81. https://doi.org/10.1177/1350650119846004.

[7]   Frene J, Nicolas D, Degueurce B, Berthe D, Godet M. Hydrodynamic lubrication: bearings and thrust bearings. Elsevier; 1997.

[8]   Wardle F. Ultra-precision bearings. Elsevier; 2015.

[9]   Bassani R. Lubricated hybrid journal bearings. J Tribol 2011;133:1–5. https://doi.org/10.1115/1.4002875.

[10]   Lampaert SGE, Quinci F, van Ostayen RAJ. Rheological texture in a journal bearing with magnetorheological fluids. J Magn Magn Mater 2020;499:1–10. https://doi.org/10.1016/j.jmmm.2019.166218.

[11]   Glavatskih S, Höglund E. Tribotronics—Towards active tribology. Tribol Int 2008;41:934–9.

[12]   Zhu X, Jing X, Cheng L. Magnetorheological fluid dampers: A review on structure design and analysis. J Intell Mater Syst Struct 2012;23:839–73. https://doi.org/10.1177/1045389X12436735.

[13]   Nikolakopoulos PG, Papadopoulos CA. Controllable high speed journal bearings, lubricated with electro-rheological fluids. An analytical and experimental approach. Tribol Int 1998;31:225–34. https://doi.org/10.1016/s0301-679x(98)00025-5.

[14]   Peng J, Zhu KEQ. Hydrodynamic characteristics of ER journal bearings with external electric field imposed on the contractive part. J Intell Mater Syst Struct 2005;16:493–9. https://doi.org/10.1177/1045389X05052312.

[15]   Ochoüski W. Sliding bearings lubricated with magnetic fluids. Ind Lubr Tribol 2007;59:252–65. https://doi.org/10.1108/00368790710820856.

[16]   Vaz N, Binu KG, Serrao P, Hemanth MP, Jacob J, Roy N, et al. Experimental Investigation of Frictional Force in a Hydrodynamic Journal Bearing Lubricated with Magnetorheological Fluid. J Mech Eng Autom 2017;7:131–4. https://doi.org/10.5923/j.jmea.20170705.01.

[17]   Lampaert SGE, Ostayen RAJ Van. Hydrostatic bearing with MR texturing. B Abstr 16th Ger Ferrofluid Work 2017;94–5.

[18]   Kumbhar BK, Patil SR, Sawant SM. Synthesis and characterization of magneto-rheological (MR) fluids for MR brake application. Eng Sci Technol an Int J 2015;18:432–8. https://doi.org/10.1016/j.jestch.2015.03.002.

[19]   Laukiavich CA, Braun MJ, Chandy AJ. A comparison between the performance of ferro- and

magnetorheological fluids in a hydrodynamic bearing. Proc Inst Mech Eng Part J J Eng Tribol 2014;228:649–66. https://doi.org/10.1177/1350650114523753.

[20] Gertzos KP, Nikolakopoulos PG, Papadopoulos CA. CFD analysis of journal bearing hydrodynamic lubrication by Bingham lubricant. Tribol Int 2008;41:1190–204. https://doi.org/10.1016/j.triboint.2008.03.002.

[21] Sharma SC, Khatri CB. Electro-rheological fluid lubricated textured multi-lobe hole-entry hybrid journal bearing system. J Intell Mater Syst Struct 2018;29:1600–19. https://doi.org/10.1177/1045389X17742731.

[22] Carlson JD. Magnetorheological fluids. Smart Mater 2008;252:17-1-17–8. https://doi.org/10.1201/b13050-2.

[23] Dhumal J, Bandgar S, Zipare K, Shahane G. Fe3O4 ferrofluid nanoparticles: synthesis and rheological behavior. Int J Mater Chem Phys 2015;1:141–5.

[24] Osman TA, Nada GS, Safar ZS. Different magnetic models in the design of hydrodynamic journal bearings lubricated with non-Newtonian ferrofluid. Tribol Lett 2003;14:211–23. https://doi.org/10.1023/A:1022869432202.

[25] Bompos DA, Nikolakopoulos PG. CFD simulation of magnetorheological fluid journal bearings. Simul Model Pract Theory 2011;19:1035–60. https://doi.org/10.1016/j.simpat.2011.01.001.

[26] Peng J, Zhu KQ. Effects of electric field on hydrodynamic characteristics of finite-length ER journal bearings. Tribol Int 2006;39:533–40. https://doi.org/10.1016/j.triboint.2005.03.017.

[27] Laun HM, Kormann C, Willenbacher N. Rheometry on magnetorheological (MR) fluids: I. Steady shear flow in stationary magnetic fields. Rheol Acta 1996;35:417–32. https://doi.org/10.1007/BF00368993.

[28] Hesselbach J, Abel-Keilhack C. Active hydrostatic bearing with magnetorheological fluid. J Appl Phys 2003;93:8441–3. https://doi.org/10.1063/1.1555850.

[29] Lampaert SGE, van Ostayen RAJ. Experimental results on a hydrostatic bearing lubricated with a magnetorheological fluid. Curr Appl Phys 2019;19:1441–8. https://doi.org/10.1016/j.cap.2019.09.004.

[30] Litwin W, Wojciech Litwin. WATER LUBRICATED MARINE STERN TUBE BEARINGS – ATTEMPT AT ESTIMATING HYDRODYNAMIC CAPACITY. Int Jt Tribol Conf 2009:1–3.

[31] Litwin W, Olszewski A. Assessment of possible application of waterlubricated sintered brass slide bearing for marine propeller shaft. Polish Marit Res 2012;19. https://doi.org/10.2478/v10012-012-0040-4.

[32] Lampaert SGE, van Ostayen RAJ. Lubrication theory for Bingham plastics. Tribol Int 2020;147:1–12. https://doi.org/10.1016/j.triboint.2020.106160.

[33] Hassan MF, Mailah M, Junid R, Alang NA. Vibration suppression of a handheld tool using intelligent active force control (AFC). Proc. World Congr. Eng., vol. 2, London (UK); 2010, p. 1636–41.

[34] Fan C-C, Pan M-C. Active elimination of oil and dry whips in a rotating machine with an electromagnetic actuator. Int J Mech Sci 2011;53:126–34.

[35] Vischer D, Bleuler H. Self-sensing active magnetic levitation. IEEE Trans Magn 1993;29:1276–81.